3D Magnetization Problems in Superconductivity: Solution by the FFT-based Method

LEONID PRIGOZHIN[1], VLADIMIR SOKOLOVSKY[2]
[1]J. Blaustein Institutes for Desert Research
[2]Physics Department
Ben-Gurion University of the Negev
Beer Sheva, ISRAEL
[1]leonid@bgu.ac.il, https://www.math.bgu.ac.il/~leonid
[2]sokolovv@bgu.ac.il, https://physics.bgu.ac.il/people/97/

Abstract: - The fast Fourier transform (FFT) based numerical method for thin film magnetization problems in type-II superconductivity has been proposed by Vestgården and Johansen [*Supercond. Sci. Technol.* Vol. 25, 2012, 104001]. Our work significantly improves the efficiency of their method and extends it to 3D magnetization problems for bulk superconductors and to stacks of flat thin superconducting films of arbitrary shape, the two configurations of interest for a variety of practical applications. The method is efficient, allows for a highly nonlinear current–voltage relation characterising the superconducting material, and is much easier to implement than the recently proposed approaches based upon the finite element methods. We present solutions to two realistic bulk problems, where superconductors are employed for magnetic shielding and as a magnetic field concentrator (a lens). A rescaled solution to a few-film-stack problem was used to obtain an accurate approximation to the anisotropic homogenization limit of magnetization of a densely packed stack of many films.

Key-Words: - Type-II superconductivity; numerical solution; 3D magnetization problems; fast Fourier transform.

1 Introduction

Macroscopically, magnetization of type-II superconductors (SC) is well described by the eddy current model with a highly nonlinear current–voltage relation. Numerical simulations based on such a model help to understand the peculiarities of magnetic flux penetration into a superconductor and are necessary to design superconductor-based devices for electronic and electric power applications. Several finite element methods where proposed for 3D magnetization problems (see, e.g., the recent works [1-2] and the references therein). Here we consider an alternative approach, extending to such problems the 2D FFT-based method [3]; for more details see our works [4-6].

2 Bulk Superconductors

2.1 Magnetic Field Formulation

Let $\Omega \subset R^3$ be the domain occupied by a superconductor, Γ - its boundary, and $\boldsymbol{j}$ - the current density satisfying $\nabla \cdot \boldsymbol{j} = 0$ in Ω and having a zero normal component, $j_{\rm n} = 0$, on Γ. For simplicity, we will restrict our consideration to the contourwise simply connected domains, assume the applied external magnetic field $\boldsymbol{h}_{\rm e}(t)$ is uniform and $\boldsymbol{j} = \boldsymbol{0}$ in $\Omega_{\rm out} = R^3 \setminus (\Omega \cup \Gamma)$. As is most often done, we assume the electric field $\boldsymbol{e}$ and the current density $\boldsymbol{j}$ in the superconductor are parallel and

$$\boldsymbol{e} = \rho(|\boldsymbol{j}|)\boldsymbol{j}, \tag{1}$$

where $\rho(|\boldsymbol{j}|) = (e_0 / j_{\rm c})|\boldsymbol{j} / j_{\rm c}|^{n-1}$ is the nonlinear resistivity, the power n and the critical current density $j_{\rm c}$ are constant, and $e_0 = 10^{-4}$ Vm^{-1}. By the Biot-Savart law

$$\boldsymbol{h} = \boldsymbol{h}_{\rm e} + \boldsymbol{\Phi}[\boldsymbol{j}], \tag{2}$$

where $\boldsymbol{\Phi}[\boldsymbol{j}] = \nabla \times \int_{R^3} G(\boldsymbol{r} - \boldsymbol{r}')\boldsymbol{j}(\boldsymbol{r}', t)\,{\rm d}\boldsymbol{r}'$, $\boldsymbol{r} = (x, y, z)$, and $G(\boldsymbol{r}) = (4\pi|\boldsymbol{r}|)^{-1}$ is the Green function.

To formulate an evolutionary problem for the magnetic field we need also the Faraday law

$$\mu_0 \dot{\boldsymbol{h}} = -\nabla \times \boldsymbol{e}, \tag{3}$$

where μ_0 is the magnetic permeability of vacuum and a dot above a variable means the time derivative. Let at time t the magnetic field $\boldsymbol{h}$ be known. Then

$$\boldsymbol{j} = \nabla \times \boldsymbol{h} \tag{4}$$

and electric field in Ω is determined by (1). However, $\boldsymbol{e}$ remains undetermined in the non-conductive domain Ω_{out} and we cannot find $\dot{\boldsymbol{h}}$ there directly from (3). This is a complication but note that $\dot{\boldsymbol{h}}$ in Ω_{out} should be such that $\dot{\boldsymbol{j}}_{\text{out}} = \nabla \times \dot{\boldsymbol{h}}|_{\Omega_{\text{out}}} = \boldsymbol{0}$. We use this condition to find $\dot{\boldsymbol{h}}|_{\Omega_{\text{out}}}$ iteratively as follows.

First, we compute $\boldsymbol{j} = \nabla \times \boldsymbol{h}$, set

$$\boldsymbol{e} = \begin{cases} \rho(\boldsymbol{j})\boldsymbol{j} & \text{in } \Omega, \\ \rho_{\text{out}}\boldsymbol{j} & \text{in } \Omega_{\text{out}}, \end{cases} \tag{5}$$

where ρ_{out} is a sufficiently high (see below) fictitious resistivity, then use (3) to find $\dot{\boldsymbol{h}}_{\text{in}} = \dot{\boldsymbol{h}}|_{\Omega}$ and an initial approximation, $\dot{\boldsymbol{h}}^0_{\text{out}} = \dot{\boldsymbol{h}}|_{\Omega_{\text{out}}}$, in Ω_{out}. On the *i*-th iteration we compute $\dot{\boldsymbol{j}}^i = \nabla \times \dot{\boldsymbol{h}}^i$, set

$$\dot{\boldsymbol{h}}^{i+1}_{\text{out}} = \dot{\boldsymbol{h}}_{\text{e}} + \boldsymbol{\Phi}[\dot{\boldsymbol{j}}^i_{\text{in}}]|_{\Omega_{\text{out}}}, \tag{6}$$

where $\dot{\boldsymbol{j}}^i_{\text{in}} = \dot{\boldsymbol{j}}^i$ in Ω and zero in Ω_{out}. Provided these iterations converge, $\dot{\boldsymbol{j}}|_{\Omega_{\text{out}}} = \nabla \times \dot{\boldsymbol{h}}|_{\Omega_{\text{out}}} = (\dot{\boldsymbol{j}}_{\text{in}})|_{\Omega_{\text{out}}} = \boldsymbol{0}$ as desired.

The operator $\boldsymbol{\Phi}$ can be expressed by means of convolutions in R^3,

$$\boldsymbol{\Phi}[\boldsymbol{j}] = \begin{Bmatrix} j_z * \partial_y G - j_y * \partial_z G \\ j_x * \partial_z G - j_z * \partial_x G \\ j_y * \partial_x G - j_x * \partial_y G \end{Bmatrix}.$$

Since the Fourier transform of G in R^3 is $F(G) = \int_{R^3} G(\boldsymbol{r}) e^{-\mathrm{i}\boldsymbol{k}\cdot\boldsymbol{r}} \mathrm{d}\boldsymbol{r} = 1/|\boldsymbol{k}|^2$, where $\boldsymbol{k} = (k_x, k_y, k_z)$, we obtain

$$\boldsymbol{\Phi}[\boldsymbol{j}] = F^{-1}\left\{ \frac{\mathrm{i}}{|\boldsymbol{k}|^2} \begin{bmatrix} k_y F(j_z) - k_z F(j_y) \\ k_z F(j_x) - k_x F(j_z) \\ k_x F(j_y) - k_y F(j_x) \end{bmatrix} \right\}. \tag{7}$$

This expression is not determined for $\boldsymbol{k} = \boldsymbol{0}$ but, taking into account that $\int_{R^3} \boldsymbol{\Phi}[\boldsymbol{j}] \mathrm{d}\boldsymbol{r} = \int_{R^3} [\boldsymbol{h} - \boldsymbol{h}_{\text{e}}(t)] \mathrm{d}\boldsymbol{r}$ should be zero at each moment in time, for $\boldsymbol{k} = \boldsymbol{0}$ we replace $1/|\boldsymbol{k}|^2$ in (7) by zero.

2.2 Numerical Scheme

To make this algorithm practical a uniform regular grid was defined in a rectangular domain containing Ω and enough empty space around it; the Fourier transform and its inverse were replaced by their discrete counterparts on this grid and the FFT algorithm employed. The spatial derivatives in (3) and (4) were also computed in the Fourier space with Gaussian smoothing; the smoothing parameter was of the order of the grid step. The spatially discretized algorithm provided an approximation to $\dot{\boldsymbol{h}}$ values in the grid nodes for a given set of $\boldsymbol{h}$ node values; the resulting system of ordinary differential equations was integrated in time by the ode23 solver of Matlab.

We note that the role of fictitious resistivity ρ_{out} is to suppress the stray current only in a thin layer near the superconductor boundary; the iterations take care of this current in the rest of Ω_{out}. Moreover, our computations showed that much faster convergence of iterations (6) is achieved if $\dot{\boldsymbol{h}}^0_{\text{out}}$ is taken as $\dot{\boldsymbol{h}}_{\text{out}}$ from the previous time step and (5) is used only for defining $\dot{\boldsymbol{h}}_{\text{in}}$ via (3).

In our simulations the virgin initial state was assumed and the power $n = 30$. We used dimensionless variables,

$$(x', y', z') = \frac{(x, y, z)}{l}, \quad t' = \frac{t}{t_0}, \qquad \boldsymbol{e}' = \frac{\boldsymbol{e}}{e_0}, \quad \boldsymbol{j}' = \frac{\boldsymbol{j}}{j_{\text{c}}}, \quad \boldsymbol{h}' = \frac{\boldsymbol{h}}{j_{\text{c}} l}, \tag{8}$$

where l is the characteristic size and $t_0 = \mu_0 j_{\text{c}} l^2 / e_0$; below, the prime is omitted.

2.3 Examples

Shielding sensitive scientific and medical devices from the magnetic field environment is one of the promising applications of superconductors. Magnetic field concentration by superconducting magnetic lenses is the opposite phenomenon based, however, on the same properties of superconductors: their ideal conductivity and ability to expel the magnetic field.

2.3.1 Example 1: Magnetic Shield

Our first example is a hollow, closed at one end superconducting cylinder (Fig. 1); its sizes are taken from [7] and scaled in accordance with (8); see [5] for the details of this simulation.

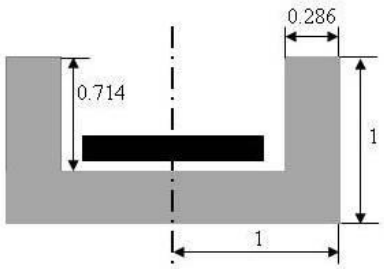

Fig.1: Scheme of the superconducting shield (gray); dimensionless units. Black area is the shielded zone.

We considered two cases. Case A: the external field first grows along the cylinder axis, then in a direction perpendicular to it: $\boldsymbol{h}_e = (0,0,t)$ for $0 \le t \le \tau$ and $\boldsymbol{h}_e = (t-\tau,0,\tau)$ for $\tau \le t \le 2\tau$ with $\tau = 0.09$. Case B: same variations in the inverse order, $\boldsymbol{h}_e = (t,0,0)$ for $0 \le t \le \tau$ and $\boldsymbol{h}_e = (\tau,0,t-\tau)$ for $\tau \le t \le 2\tau$. To illustrate the shielding performance, we compared the applied field magnitude $|\boldsymbol{h}_e|$ with the mean magnitude $\langle|\boldsymbol{h}|\rangle$ of the magnetic field inside the "shielded zone" defined as a disk, co-axial to the cylinder (Fig. 1). Because the cylinder is short, fields perpendicular to its axis penetrate the shielded zone much easier than a field parallel to this axis, see Fig. 2.

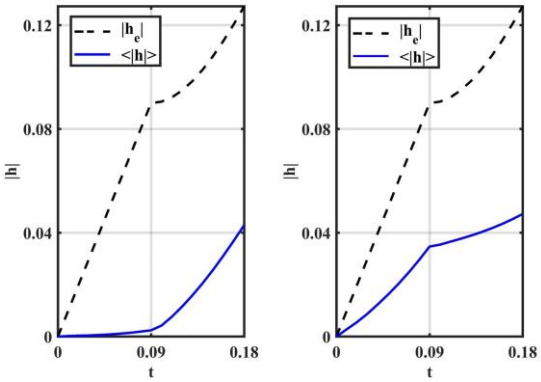

Fig.2: Shielding performance, different variations of the external field: left - case A, right - case B. Dashed line - the applied field magnitude, solid line - the average magnetic field magnitude in the shielded zone.

We present also the calculated distributions of the magnetic field and current density for the case A at $t = \tau$ and $t = 2\tau$ (Fig. 3).

2.3.2 Example 2: Magnetic lens

The magnetic lens in our second example (Fig. 4) is geometrically similar to those studied experimentally in [8]: it is a superconducting cylinder with a coaxial biconical hole and a narrow slit to prevent the shielding circumference current; see [5] for a detailed exposition. The applied field was parallel to the cylinder axis, $\boldsymbol{h}_e = (0,0,t)$, $0 \le t \le 0.2$. Partially expelled from the superconductor, magnetic field was concentrated in the central part of the lens. The average field magnitude in the central region $\{r \le 0.2,\ |z| \le 0.33\}$ was about twice higher than the applied field for $|\boldsymbol{h}_e| = 0.05$ and 1.6 times higher for $|\boldsymbol{h}_e| = 0.2$ (Fig. 5). In dimensional units for, e.g., a lens with the outer diameter 30 mm and the critical current density 5×10^8 A/m^2, the field of 0.473 T is amplified twice and of 1.89 T – 1.6 times. The computed current density and magnetic field distributions are presented in Fig. 6 for $t = 0.1$ and $t = 0.2$.

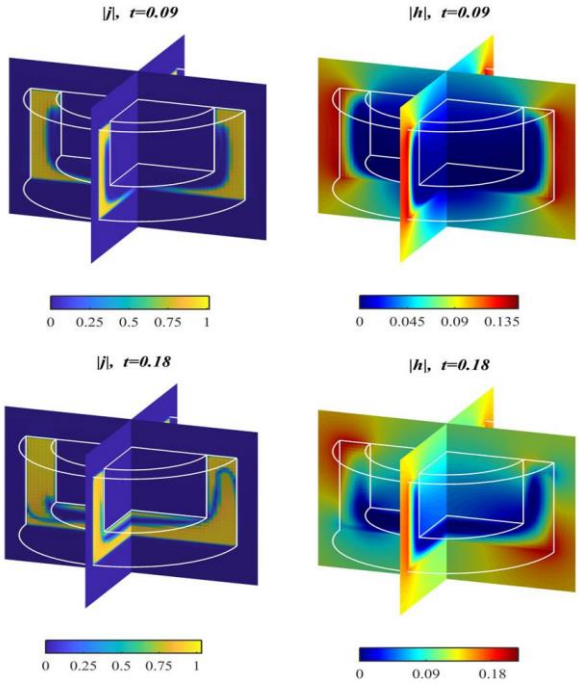

Fig.3: Magnetic shield simulation (case A). Magnitudes of the current density (left) and magnetic field (right) in the cross-sections $x = 0$ and $y = 0$.

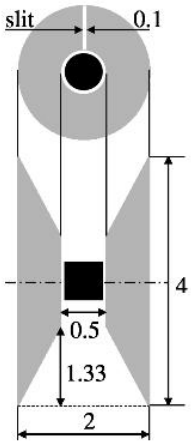

Fig.4: Scheme of the magnetic lens (gray) and the lens central region (black).

3 Stacks of Thin Superconducting Films

Progress in fabrication and commercial availability of high temperature coated conductors made stacks of such conductors an attractive alternative to bulk superconductors for trapping

strong magnetic fields, magnetic levitation, etc. Advantages of coated conductors are their high critical current density, better mechanical and thermal stability due to the metal substrate layers, higher degree of uniformity, and flexibility in adaptation to different configurations.

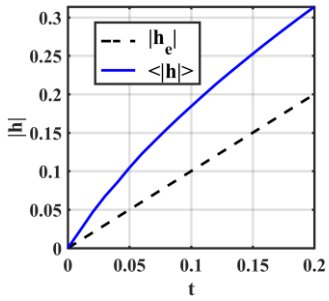

Fig.5: Dashed line - the applied field magnitude, solid line - the average magnetic field magnitude in the magnetic lens central region.

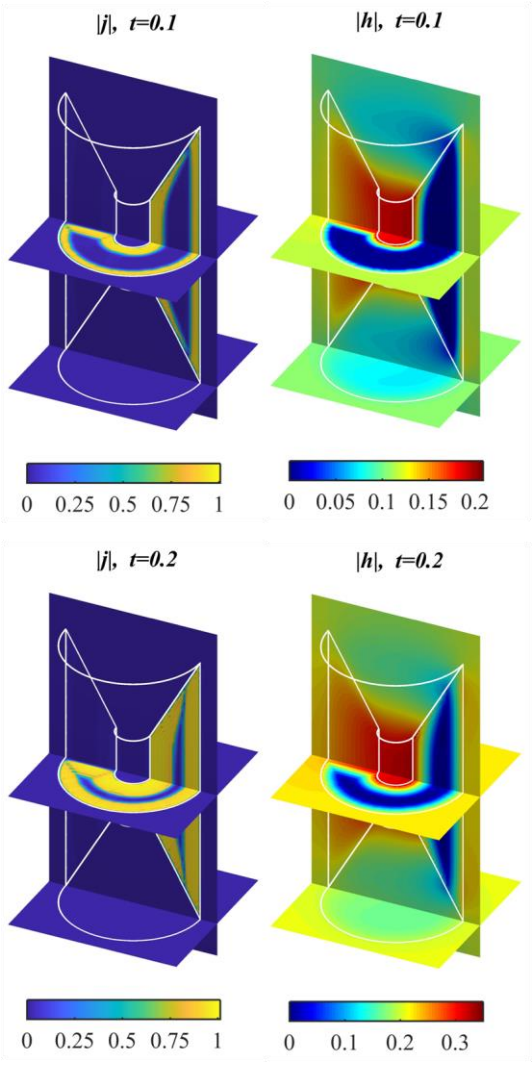

Fig.6: Magnetic lens. Magnitudes of the current density (left) and magnetic field (right) in the cross-sections $x=0$, $z=0$, and $z=-2$.

Stacks of coated conductors experience much weaker crossed field demagnetization; this property is important for the superconducting magnets in electric machines.

Typically, the width to thickness ratio of the superconducting layer in coated conductors is between 1000 and 10000, which justifies modeling using the infinitely thin film approximation.

3.1 Stream Function Formulation

Let us consider a stack of N thin equidistant superconducting films,

$$\{(x,y,z_m):(x,y)\in\Omega,\ z_m=md\},\quad m=1,...,N,$$

where d is the distance between films. For simplicity, we assume that the domain $\Omega\subset R^2$ is simply connected, the normal to films z-component of the applied magnetic field is uniform, $h_{e,z}=h_{e,z}(t)$, and in all films the same power law,

$$\boldsymbol{e}_m=\rho(|\boldsymbol{j}_m|)\boldsymbol{j}_m=e_0\left(\frac{|\boldsymbol{j}_m|}{j_c}\right)^{n-1}\frac{\boldsymbol{j}_m}{j_c}, \qquad (9)$$

holds for the *sheet* current densities, $\boldsymbol{j}_m$, and the parallel to films electric field components, $\boldsymbol{e}_m$. As above, $e_0=10^{-4}$ V/m, the sheet critical current density j_c and the power n are assumed constant. Since $\nabla\cdot\boldsymbol{j}_m=0$ in Ω and the normal component of $\boldsymbol{j}_m$ on the domain boundary Γ is zero, there exist stream functions g_m such that $\boldsymbol{j}_m=\bar{\nabla}\times g_m$ (i.e. $j_{m,x}=\partial_y g_m$, $j_{m,y}=-\partial_x g_m$) and $g_m|_\Gamma=0$. Let us extend g_m by zero to the outer domain $\Omega_{out}=R^2\setminus(\Omega\bigcup\Gamma)$ and define $G_{m-l}(\boldsymbol{r})=\left(4\pi\sqrt{r^2+d^2(m-l)^2}\right)^{-1}$, where $\boldsymbol{r}=(x,y)$ and $r=|\boldsymbol{r}|$. By the Biot-Savart law

$$h_{m,z}-h_{e,z}=\sum_{l=1}^{N}\nabla\times\int_\Omega G_{m-l}(\boldsymbol{r}-\boldsymbol{r}')\boldsymbol{j}_l(\boldsymbol{r}',t)d\boldsymbol{r}'$$

$$=\sum_{l=1}^{N}\bar{\nabla}\times G_{m-l}*\bar{\nabla}\times g_l$$

$$=-\sum_{l=1}^{N}\left(\partial_x G_{m-l}*\partial_x g_l+\partial_y G_{m-l}*\partial_y g_l\right),$$

where $\nabla\times\boldsymbol{u}=\partial_x u_y-\partial_y u_x$ is the scalar 2D curl of a vector function, $h_{m,z}$ is the z-component of magnetic field on the m-th film, and $*$ denotes the 2D convolution. Applying the Fourier transform

$F[f]=\int_{R^2} f(\boldsymbol{r})e^{-i\boldsymbol{kr}}\mathrm{d}\boldsymbol{r}$ we obtain $F\left[h_{m,z}-h_{\mathrm{e},z}\right]=k^2\sum_{l=1}^{N}F[G_{m-l}]F[g_l]$, where $k^2=k_x^2+k_y^2$. For $k\neq 0$ this yields a linear algebraic system for $F[g_l]$, $l=1,...,N$:

$$\sum_{l=1}^{N}F[G_{m-l}]F[g_l]=\frac{1}{k^2}F[h_{m,z}-h_{\mathrm{e},z}]. \quad (10)$$

Since $F[G_{m-l}](\boldsymbol{k})=(2k)^{-1}e^{-kd|m-l|}$ (see [6]), we rewrite (10) as

$$\sum_{l=1}^{N}A_{m,l}(k)F[g_l](\boldsymbol{k})=\frac{2}{k}F[h_{m,z}-h_{\mathrm{e},z}](\boldsymbol{k}),$$

where $A_{m,l}(k)=q^{|m-l|}$ with $q(k)=e^{-kd}$. For $k\neq 0$ the symmetric $N\times N$ matrix $\boldsymbol{A}$ has a simple three-diagonal inverse:

$$\boldsymbol{A}^{-1}(k)=\frac{1}{1-q^2}\begin{pmatrix} 1 & -q & 0 & ... & & 0\\ -q & q^2+1 & -q & 0 & ... & 0\\ 0 & -q & q^2+1 & -q & ... & 0\\ & & ... & & & \\ 0 & ... & 0 & -q & q^2+1 & -q\\ 0 & ... & & 0 & -q & 1 \end{pmatrix}.$$

Hence, if the functions $F[h_m-h_{\mathrm{e},z}]$ are known, the functions $F[g_m]$ remain undetermined only for $k=0$. These values correspond to additive constants in the real space and we express $\boldsymbol{g}=(g_1,...,g_N)^T$ as

$$\boldsymbol{g}=\boldsymbol{\Phi}[\delta\boldsymbol{h}_z]:=F^{-1}\left[\frac{2}{k}\boldsymbol{A}^{-1}(k)F[\delta\boldsymbol{h}_z]\right]-\boldsymbol{C}(t) \quad (11)$$

where $\delta\boldsymbol{h}_z=(h_{1,z}-h_{\mathrm{e},z},...,h_{N,z}-h_{\mathrm{e},z})^T$, $\frac{2}{k}\boldsymbol{A}^{-1}(k)$ is replaced by the zero matrix for $k=0$, $\boldsymbol{C}=(C_1,...,C_N)^T$, and at each moment in time the shifts $C_m(t)$ are chosen to satisfy the conditions $\int_{\Omega_{\mathrm{out}}}g_m\mathrm{d}\boldsymbol{r}=0$. Differentiating (11), we obtain

$$\dot{\boldsymbol{g}}=\boldsymbol{\Phi}[\delta\dot{\boldsymbol{h}}_z]=F^{-1}\left[\frac{2}{k}\boldsymbol{A}^{-1}(k)F[\delta\dot{\boldsymbol{h}}_z]\right]-\dot{\boldsymbol{C}} \quad (12)$$

with $\dot{\boldsymbol{C}}$ such that $\int_{\Omega_{\mathrm{out}}}\dot{\boldsymbol{g}}\mathrm{d}\boldsymbol{r}=\boldsymbol{0}$. We can now formulate an evolutionary problem for $\boldsymbol{g}$. Let all stream functions g_m be known at time t. Then we also know the sheet current densities $\boldsymbol{j}_m=\bar{\nabla}\times g_m$ and can find the parallel to films electric field components in each film using (9). By the Faraday law we have

$$\dot{h}_{m,z}=-\mu_0^{-1}\nabla\times\boldsymbol{e}_m=\mu_0^{-1}\nabla\cdot\left[\rho(|\nabla g_m|)\nabla g_m\right].$$

This does not determine the evolutionary problem via (12) yet because the electric fields $\boldsymbol{e}_m$ and, hence, $\dot{h}_{m,z}$ and $\delta\dot{\boldsymbol{h}}_z$ in Ω_{out} remain unknown. However, in the outer domain $\boldsymbol{g}$ should remain zero, which is an implicit condition for $\delta\dot{\boldsymbol{h}}_z|_{\Omega_{\mathrm{out}}}$: equation (12) should hold with $\dot{\boldsymbol{g}}|_{\Omega_{\mathrm{out}}}=\boldsymbol{0}$. This condition can be resolved iteratively. It may be noted that the known formulation for a single film magnetization problem is obtained for $N=1$ in the $d\to+\infty$ limit.

3.2. Iterations

To find the derivative $\dot{\boldsymbol{g}}$ for a given $\boldsymbol{g}$, we find $\boldsymbol{j}_m=\bar{\nabla}\times g_m$ for each film and set, as in the bulk case,

$$\boldsymbol{e}_m=\begin{cases}\rho(|\boldsymbol{j}_m|)\boldsymbol{j}_m & \text{in } \Omega,\\ \rho_{\mathrm{out}}\boldsymbol{j}_m & \text{in } \Omega_{\mathrm{out}}\end{cases}$$

with a sufficiently high constant fictitious resistivity ρ_{out}. Then we define $\dot{h}_{m,z}^{(0)}=-\mu_0^{-1}\nabla\times\boldsymbol{e}_m$, $\delta\dot{h}_{m,z}^{(0)}=\dot{h}_{m,z}^{(0)}-\dot{h}_{\mathrm{e},z}$, and set an initial approximation $\dot{\boldsymbol{g}}^{(0)}=\boldsymbol{\Phi}[\delta\dot{\boldsymbol{h}}_z^{(0)}]$. On the *i*-th iteration, we improve $\dot{h}_{m,z}^{(i)}$ by subtracting the time derivative of the field induced at $z=md$ by the stray current outside the film. For normal to the m-th film component of this field the derivative can be presented as $F^{-1}\left[(k/2)F[\dot{g}_{m,\mathrm{out}}]\right]$, where

$$\dot{g}_{m,\mathrm{out}}=\begin{cases}0 & \text{in } \Omega,\\ \dot{g}_m & \text{in } \Omega_{\mathrm{out}}.\end{cases}$$

The values of $\dot{h}_{m,z}$ in the film itself are determined by the Faraday law and for all m we update $\dot{h}_{m,z}$ only in Ω_{out} setting

$$\dot{h}_{m,z}^{(i+1)}|_{\Omega_{\mathrm{out}}}=\dot{h}_{m,z}^{(i)}|_{\Omega_{\mathrm{out}}}-\lambda F^{-1}\left[(k/2)F[\dot{g}_{m,\mathrm{out}}^{(i)}]\right]\Big|_{\Omega_{\mathrm{out}}}-D_m^{(i)},$$

where the shifts $D_m^{(i)}$ ensure the conditions $\int_{R^2}\left(\dot{h}_{m,z}^{(i+1)}-\dot{h}_{\mathrm{e},z}\right)\mathrm{d}\boldsymbol{r}=0$ and λ is a relaxation parameter, then find $\dot{\boldsymbol{g}}^{(i+1)}=\boldsymbol{\Phi}[\delta\dot{\boldsymbol{h}}_z^{(i+1)}]$.

Provided these iterations converge, $\dot{g}_{m,\mathrm{out}}^{(i)}$ tend to zero for all m as desired.

3.3 Implementation

The film stack computations were performed on a regular grid defined in a rectangle containing and several times larger than Ω. As in the bulk case, the convolutions and derivatives were computed in the Fourier space using the FFT. The fictitious resistivity ρ_{out} should suppress currents only in a thin boundary layer and, usually, does not need to be very high. The simulations (see [6]) were performed in dimensionless variables with the relaxation parameter λ proportional to d/l, where l is the characteristic film size. A faster convergence of iterations was obtained with $\dot{h}_{m,z}^{(0)}|_{\Omega_{\mathrm{out}}}$ taken as $\dot{h}_{m,z}|_{\Omega_{\mathrm{out}}}$ from the previous time step. The ordinary differential equations for the grid values of $\boldsymbol{g}$ were integrated in time by the Matlab solver ode23.

3.4 Homogenization

Employed in applications are often stacks of several hundreds of densely packed coated conductors. In such cases an accurate solution to magnetization problems can be obtained using homogenization and transition to the anisotropic bulk model [9-11]. The stack of N films with the distance d between films and the current-voltage relation (9) is replaced by a cylindrical bulk superconductor of the height $H=Nd$ and cross-section Ω, characterized by the infinite resistivity in the *z*-axis direction and the power current-voltage law for the parallel to *xy*-plane component $\boldsymbol{e}$ of the electric field and the bulk current density $\boldsymbol{J}$. Here the critical current density $J_{\mathrm{c}}=j_{\mathrm{c}}/d$ equals the film sheet critical current density averaged over the layer of thickness d.

$$\boldsymbol{e}=e_{\mathrm{c}}\left(\frac{|\boldsymbol{J}|}{J_{\mathrm{c}}}\right)^{n-1}\frac{\boldsymbol{J}}{J_{\mathrm{c}}}$$

For the fixed parameters J_{c} and H the anisotropic bulk model solution is the limit of solutions to stack problems with the sheet critical current densities $j_{\mathrm{c}}^N=J_{\mathrm{c}}d_N=J_{\mathrm{c}}H/N$ as the number of films N tends to infinity. Using several different finite element methods, magnetization of such initially non-magnetized anisotropic bulk $10\times10\times1$ mm^3 superconductor was simulated in [2, 12] for the critical current density $J_c=10^8$ Am^{-2}, the power $n=25$, and the sinusoidal applied field $h_{\mathrm{e},z}$ with the amplitude 100 mT and frequency 50 Hz. Presented in these works are, in particular, the current density distribution at the first peak of the applied field, $t=0.25T$, where T is the period, and the AC loss, $Q=-\mu_0\int m_z\mathrm{d}h_{\mathrm{e},z}$, computed for the cycle $0.25T\le t\le1.25T$; here m_z is the *z*-component of the magnetic moment. The loss values obtained by different finite element methods in [2,12] varied from 3.45 to 3.50 mJ, the computations on a personal computer took from 1.7 to 6 days [12].

Since it turned difficult to solve this benchmark problem using the 3D FFT-based method for an anisotropic superconductor having a resistivity in *z*-direction fully suppressing the corresponding current component, we used a different approach, suggested for two-dimensional problems (stacks of long strips) in [11]. As was noted there, if the ratio of the film distance d to the half of superconducting strip width is less than 0.05, the difference between the AC losses in a stack and the corresponding anisotropic bulk superconductor does not exceed 2%. Hence, instead of the full homogenization and transition to the anisotropic bulk model, it is possible to replace the densely packed N-film stack by a stack with a lower number of tapes, $N_0\ll N$, the same height $H=dN=d_0N_0$, and the new sheet critical current density $j_{\mathrm{c},0}=d_0J_c=d_0j_{\mathrm{c}}/d$.

For the stack benchmark problem [2,12], the ratio of stack height to the film half-side a is 0.2. With only 4 films we already have $d/a=0.05$ and so even the 4-film stack should be a good approximation to the benchmark problem. Since the normal to film component of the magnetic moment can be conveniently expressed via the stream function, $m_z=\frac{1}{2}\int_\Omega\boldsymbol{r}\times\boldsymbol{j}\mathrm{d}\boldsymbol{r}=\int_\Omega g\,\mathrm{d}\boldsymbol{r}$, the AC loss per period for the film stacks was calculated as

$$Q=-\int_{0.25T}^{1.25T}\dot{h}_{\mathrm{e},z}\left(\sum_{l=1}^{N}\int_\Omega g_l\mathrm{d}\Omega\right)\mathrm{d}t.$$

Our computations on a similar personal computer were faster than those in [12]; the computed AC losses coincided with those in other works within 1-2% (see Tab. 1).

Table 1. Computation results

N of films	Q, mJ	Computation time, hours
4	3.43	9
6	3.51	23

We present also the distributions of calculated sheet current densities $\boldsymbol{j}_m$ in a 6-film stack (Fig. 7) and the approximation to the current density $\boldsymbol{J}$ in the anisotropic bulk, obtained for this stack as $\boldsymbol{J} = \boldsymbol{j}_m / d$ at $z = z_m$ (Fig. 8). The latter distribution is very similar to those in [2,12].

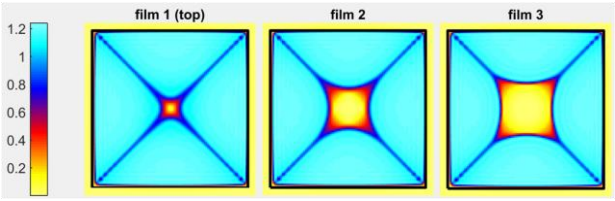

Fig.7: Scaled sheet current densities $|\boldsymbol{j}_m| / j_{c,0}$ in three upper films of a 6-film stack at the peak of the applied field.

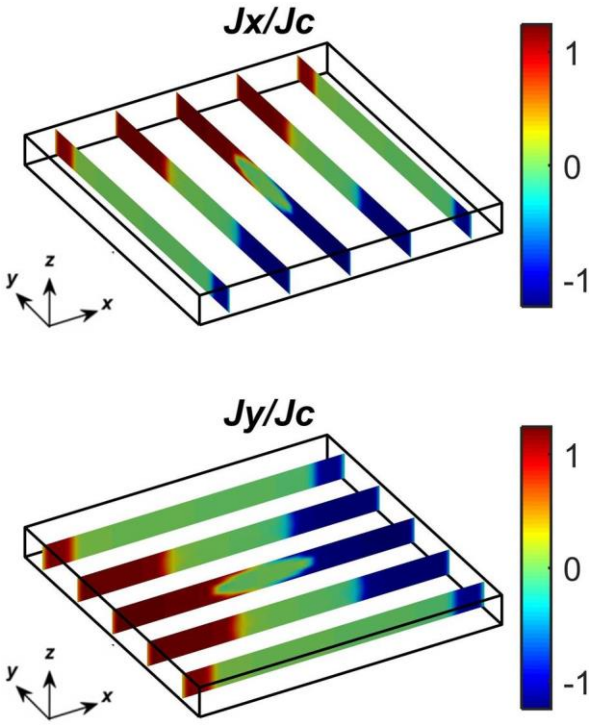

Fig.8: Current density at the peak of applied field: solution of the anisotropic bulk benchmark problem computed using the 6-film stack approximation.

4 Conclusion

Numerical solution of highly nonlinear 3D magnetization problems in type-II superconductivity is currently an active area of research. The FFT-based method considered in our work is, for such problems, an alternative to more popular finite element methods. Our simulations showed that the FFT-based method is efficient and general: it can be successfully employed not only to solving the thin film magnetization problems but also for modeling bulk superconductors of realistic geometries and thin film stacks. The method is simpler and, at least in some cases, faster than its recently developed finite element competitors.

Although in our examples we used only a power current–voltage relation with constant power and critical current density, it can be replaced by a more realistic field-dependent relation.

References:

[1] E. Pardo and M. Kapolka, 3D computation of non-linear eddy currents: Variational method and superconducting cubic bulk, *J. Comp. Physics*, Vol. 344, 2017, pp. 339-363.

[2] M. Olm, S. Badia and A.F. Martín, Simulation of high temperature superconductors and experimental validation, *Computer Phys. Communications*, Vol. 237, 2019, pp. 154-167.

[3] J.I. Vestgården and T.H. Johansen, Modeling non-local electrodynamics in superconducting films: the case of a right angle corner, *Supercond. Sci. Technol.* Vol. 25, No.10, 2012, 104001.

[4] L. Prigozhin and V. Sokolovsky, Fast Fourier transform-based solution of 2D and 3D magnetization problems in type-II superconductivity, *Supercond. Sci.Technol.* Vol. 31, No.5, 2018, 055018.

[5] L. Prigozhin and V. Sokolovsky, 3D simulation of superconducting magnetic shields and lenses using the fast Fourier transform, *J. Appl. Physics*, Vol. 123, No. 23, 2018, 233901.

[6] L. Prigozhin and V. Sokolovsky, Solution of 3D magnetization problems for superconducting film stacks, *Supercond. Sci. and Technol.* Vol. 31, No.12, 2018, 125001.

[7] L. Gozzelino, R. Gerbaldo, G. Ghigo, F. Laviano, M. Truccato, A. Agostino, Superconducting and hybrid systems for magnetic field shielding, *Supercond. Sci. Technol.* Vol. 29, No.3, 2016, 034004.

[8] Z.Y. Zhang, S. Choi, S. Matsumoto, R. Teranishi, G. Giunchi, A.F. Albisetti, T.

Kiyoshi, Magnetic lenses using different MgB_2 bulk superconductors, *Supercond. Sci. Technol.* Vol. 25, No.2, 2012, 025009.

[9] J. R. Clem, J.H. Claassen and Y. Mawatari, AC losses in a finite Z stack using an anisotropic homogeneous-medium approximation, *Supercond. Sci. Technol.* Vol. 20, No.12, 2007, pp. 1130-1139.

[10] Y. Weijia, A.M. Campbell, and T.A. Coombs, A model for calculating the AC losses of second-generation high temperature superconductor pancake coils, *Supercond. Sci. Technol.* Vol. 22, 2009, 075028.

[11] L. Prigozhin and V. Sokolovsky, Computing AC losses in stacks of high-temperature superconducting tapes, *Supercond. Sci. Technol.* Vol. 24, No.7, 2011, 075012.

[12] M. Kapolka, V.M.R. Zermeño, S. Zou, A. Morandi, P.L. Ribani, E. Pardo, F. Grilli, Three-dimensional modeling of the magnetization of superconducting rectangular-based bulks and tape stacks, *IEEE Trans. Applied Supercond.* Vol. 28, No.4, 2018, pp. 1-6.